Development of High-performance FBG Sensor Monitor AR4041A/AR4011A

Masaru Koshihara, Kenichi Nakamura, Noriaki Yamasaki, Takanori Saitoh, Hiroshi Furukawa

[Summary] We developed a high-performance Fiber Bragg Grating (FBG) sensor monitor for strain and temperature measurements. The new FBG sensor monitor is composed of a novel wavelength-swept light source that sweeps wavelengths with single-mode lasing in the range of 110 nm and a sweep frequency of 1.25 kHz. The FBG sensor monitor can measure FBG wavelengths with a stability of 0.08 pm (corresponds to 0.064 με) and a measurement frequency of 1.25 kHz in the range between 1510 and 1590 nm.

1 Introduction

With the construction of high buildings and bridges, etc., in recent years, the importance of structural health monitoring technologies to assess building safety is being re-examined. In previous systems using electrical strain sensors, every sensor required a power supply and the installed sensors were easily affected by electromagnetic noise, thunderstorms, etc., causing noise components in the electrical signal measured by remote sensing and presenting a risk of degraded accuracy.

Optical fibers have been used as sensors to solve these problems with a focus on optical sensing technology. Since optical sensing technology does not require supplying power to the sensor itself, it offers many advantages including long life spans with excellent corrosion resistance[1], excellent explosion-proofness, easy remote measurement at distances of more than 10 km with no concerns about electromagnetic noise effects, etc. In addition, the characteristics of optical fibers lends them to linear and sheet designs for extreme environments, making them ideal for disaster monitoring and structural health monitoring systems.

Some of the well-known technologies in optical fiber sensing rely on measuring changes in the frequency of Brillouin backscatter occurring in optical fibers to determine structural deformations and temperature changes (Brillouin Optical Time Domain Reflectometer (BOTDR)), and measuring changes in the intensity of Raman scattering to determine temperature changes (Raman Optical Time Domain Reflectometer (ROTDR). Another method uses a Fiber Bragg Grating (FBG) forming a diffraction grating at the optical fiber core as a sensor to measure changes in the center wavelength of the optical spectrum reflected from the FBG sensor as an index of the amount of strain impressed on the fiber, and temperature changes.

Comparing the BOTDR and ROTDR methods to measurement methods using an FBG sensor, the former use commercially available optical fibers as the sensor without any special processing, permitting construction of relatively low-cost monitoring systems. However, because the sensor is long, the measurement distance resolution is poor. In addition, capturing the minute changes in the reflected light requires averaging of measured data and filter processing, so measurement requires times ranging from several tens of seconds to several minutes. As a consequence, the required real-time measurement is not achieved.

On the other hand, if it is possible to assure the dynamic range of the reflected spectrum, measurement methods using an FBG sensor can support real-time measurement relatively easily. Furthermore, installing many general-purpose 10-mm long FBG sensor gages along the optical fiber in series both improves the measurement distance resolution and supports strain and temperature change measurements over a wide range. Due to these many advantages, methods using FBG sensors have been adopted for monitoring large structures such as high bridges and dams[1,2], monitoring river levels after cloudbursts[3], detecting landslips[4], detecting intruders at airports[5], and

monitoring the arrival of tsunami waves[6], etc.

We have previously developed the SF3041A/SF3011A FBG Sensor Monitor (commercial launch in 2007) using an FBG for measuring strain and temperature change[7–13]. This equipment is constructed from a wavelength swept light source (WSLS) composed of an external resonator with a MEMS scanning mirror (MEMS: Micro Electro Mechanical Systems) formed from a silicon wafer, and an optical receiver, and a signal processing circuits for controlling the WSLS and processing the measured data. This equipment inputs the wavelength swept light via an optical fiber to the FBG sensor and measures the reflected spectrum and its center wavelength by detecting the reflected light with the optical receiver.

In a FBG sensor monitoring system using a WSLS, the measurement accuracy of the FBG sensor center wavelength depends on the wavelength fluctuation of the built-in WSLS and changes in the output optical power. The sweep characteristics of the WSLS are broadly linear in the range of the spectrum width (<0.1 mm) reflected from the FBG sensor and the amount of fluctuation is extremely small. Conversely, variations in the optical output power caused by the internal mode of the WSLS have a large effect on the wavelength measurement accuracy. The WSLS in our previously developed FBG sensor monitor oscillated in multimodes and had large variations in optical output power. As a result, the strain measurement accuracy was about 2 to 3 με, which was lower than the measurement accuracy (about 1 με) of general electrical-type strain measurement systems. Moreover, since the oscillation spectrum width during sweeping is about 0.1 nm, which is about the same reflected spectral width as a commercial FBG sensor, the measured spectrum width was wider than the actual spectrum width.

More recently, we have developed a new WSLS that can sweep wavelengths over 100 nm with single-mode lasing and higher speeds[14]. This WSLS has small variations in output power and features a narrow oscillation spectrum width, during sweeping. This paper describes the development of the new AR4041A/AR4011A FBG Sensor Monitor using this new single-mode WSLS and presents some good evaluation measurement results.

2 Development Concept

Since FBG sensor monitors are used mainly for natural disaster and structural health monitoring they are designed to be convenient for installation, small and lightweight. Additionally, to be able to measure small strain and temperature changes quickly, they require a high responsivity of better than 1 kHz as well as better measurement accuracy than commercially available FBG sensor monitors and our previously developed model. With respect to the FBG sensor monitor control program, we placed heavy importance on compatibility with our previously developed model control program so that customers with the earlier system would be able to transition smoothly to the new system. The control program was developed to run on PCs using the Windows XP, Windows Vista, and Windows 7 operating systems.

3 Single Mode Wavelength Sweep Light Source

3.1 Oscillation Principle

Figure 1 shows the structure and external view of the developed single-mode WSLS. This WSLS is composed of a Littmann type external resonator with a semiconductor laser diode (LD), diffraction grating, and electromagnetically actuated MEMS scanning mirror.

The light output from the LD to the mirror is split at a diffraction grating. The diffraction grating side of the LD is covered with a antireflection coating to suppress the internal mode created within the LD. The light split by the diffraction grating is reflected by the MEMS scanning mirror and is led back down the reverse path to once again return to the LD. The isolator side of the LD is covered by a low-reflection coating, forming an optical resonator between the MEMS scanning mirror. The MEMS scanning mirror rotates back and forth about a center pivot actuated by an alternating magnetic field generated by electromagnet.

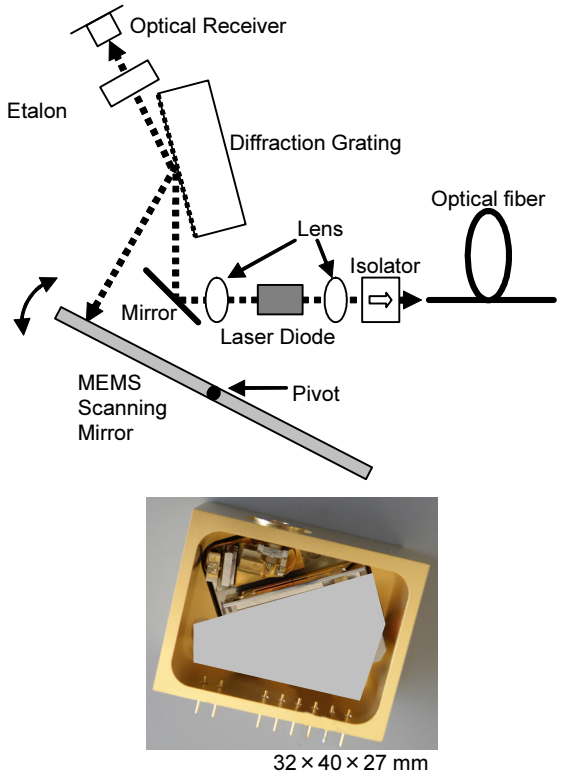

Figure 1 Schematic diagram and overview of single-mode wavelength swept light source (WSLS).

This back and forth rotation repeatedly sweeps the wavelength in a sine wave form due to the change in the external resonator length (Figure 2).

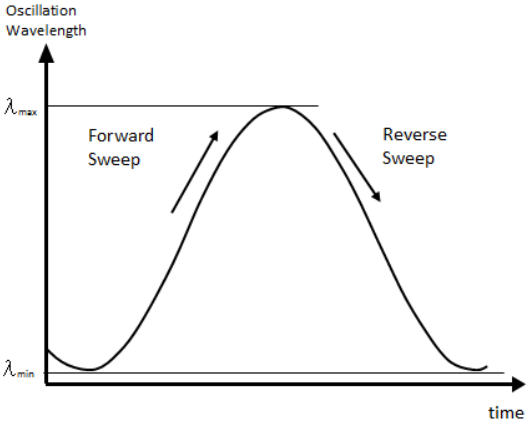

Figure 2 Lasing wavelength change of single-mode WSLS during wavelength sweeping

Since the MEMS scanning mirror rotates using a mechanical resonance, the rotation angle changes according to a sine wave form. As a result, the oscillation wavelength is also swept in a sine wave form at the same frequency. The MEMS scanning mirror resonance frequency was designed so that the sweep frequency is 1.25 kHz. The light output from the end face of the LD with the low-reflection coating passes through lenses and isolator to be supplied to the optical fiber for output.

At single-mode oscillation of the laser in the external resonator structure with the diffraction grating, the external resonator mode interval must be wide relative to the wavelength selection width of the diffraction grating. The external resonator mode interval is inversely proportional to the optical resonator length between the LD and the MEMS scanning mirror. As a result, this WSLS supports a shorter optical resonator length due to the smaller size of the optical source itself and attains the single-mode lasing due to the wider external resonator mode interval. In addition, matching the rate of change of the diffraction grating wavelength selectivity corresponding to the MEMS scanning mirror rotation angle with the rate of change of the external mode resonator wavelength determined by the optical path length from the LD to the MEMS scanning mirror achieves a configuration without mode hopping over the whole oscillation wavelength band. Moreover, the sweep wavelength band of this WSLS is 1550 nm, which is ideal for an FBG sensor.

Internally, this WSLS is designed with a wavelength monitoring function. In this wavelength monitoring function, the 0-order light from the diffraction grating is input to an etalon with a free spectrum range of 5 nm and the oscillation wavelength during sweeping is calculated by detecting the transmittance profile from this etalon at the optical receiver.

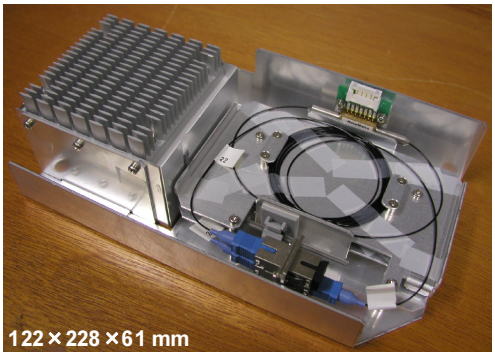

Figure 3 Overview of conventional multi-mode WSLS

The entire optical system is enclosed in a metal chassis of 32 × 40 × 27 mm and is temperature stabilized using a Peltier element. Figure 3 shows an external view of the conventional multimode WSLS. It is 122 × 228 × 61 mm in size, whereas the newly developed single-mode WSLS is just 1/50th the size of the conventional model.

3.2 Evaluating Oscillation Spectrum during Sweeping

As described previously, when this WSLS is used in an FBG sensor monitor, variation in the amplitude in the output optical power and the oscillation spectrum width during sweeping are important items, so we measured these characteristics of this WSLS. Here, we evaluated a single-mode WSLS with a sweep frequency of 1.45 kHz but since the characteristics for other sweep frequencies are the same as the 1.25 kHz sweep frequency of this WSLS, it was also used for subsequent measurements.

First, we measured the oscillation spectrum of this WSLS during sweeping using an optical spectrum analyzer; the results are shown in Figure 4. The x-axis is the wavelength and the y-axis is the optical output power. In this measurement, the sweep speed of the WSLS is faster than the optical spectrum analyzer measurement sweep speed, so the observed spectrum is trapezoidal. Here, asynchronous measurement was performed using a 10-Hz video bandwidth and a measurement resolution of 0.07 nm to assure stable measurement.

From the results, the wavelength sweep range is 110 nm from 1492 to 1602 nm. In addition, both sides of the 1550-nm center sweep wavelength have a strong output power. Since the oscillation wavelength of this WSLS changes as a sine wave, the sweep speed near the sweep return point becomes 0 and the time that the light is received by the optical spectrum analyzer becomes longer at wavelengths near this point, explaining why a stronger optical power is observed. Although the optical output fluctuation seems to be about 2 to 3 dB within the sweep range, the true power fluctuation is about 0.1 dB, because we were unable to obtain synchronization between this WSLS and the optical spectrum analyzer sweep as described later.

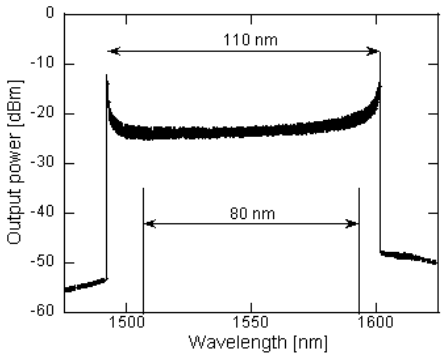

Figure 4 Spectrum of single-mode WSLS

When observing the output light at a sweep width of 110 nm with an optical spectrum analyzer set to a measurement resolution of 0.07 nm, the measured result is about 32 dB (= $10\times\log_{10}(0.07/110$ nm)) smaller than the actual output power. In this measurement result, the actual output power during sweeping can be estimated to be about 10 dBm because the power near the 1550-nm wavelength is about –23 dBm.

When applying this WSLS to an FBG sensor monitor, since the sweep wavelength changes as a sine wave as shown in Figure 2, the wavelength at both sides of the sweep range does not change linearly with respect to time. Consequently, the wavelength linearity is degraded and there is a deterioration in the accuracy for determining the wavelength reflected from the FBG sensor. As a result, when applying this WSLS to an FBG sensor monitor, the light in the wavelength band swept repeatedly near 1492 and 1602 nm is not used and only the 80-nm output light band between 1510 and 1590 nm, which is broadly linear with respect to time, is swept.

3.3 Evaluating Output Optical Power

Next, we measured the optical output power wavelength dependency from 1510 to 1590 nm. In this measurement, we measured the light output from the WSLS using the internal monitor function of the FBG sensor monitor when the WSLS was built into the FBG sensor monitor as described later. Figure 5 shows the measured results. The x-axis is wavelength and the y-axis is optical output power. The optical output power was more than 10 dBm over the whole wavelength range and the difference between the

maximum and minimum values was about 1.5 dB. Moreover, since there was no discontinuity in output power during sweeping, we confirmed that there was no mode hopping. There were some small fluctuations in the optical output power, but since the amplitude was only about 0.1 dB, the WSLS was evaluated as being sufficiently applicable to the FBG sensor monitor.

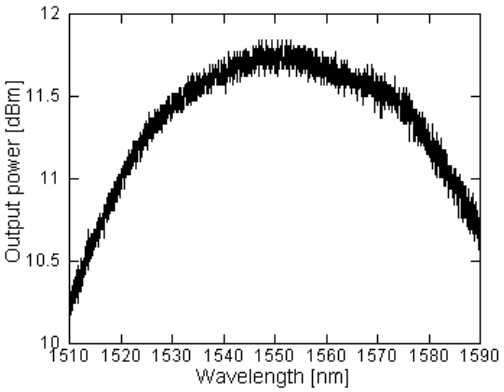

Figure 5 Wavelength dependence of optical output power for single-mode WSLS

Figures 6 (a) and (b) compare the variations in optical power with elapsed time of the conventional multimode WSLS and this newly developed WSLS. The measured wavelength was the center wavelength of the sweep frequency range for each WSLS (1570 nm for the multimode WSLS and 1550 nm for the new WSLS). The x-axis is elapsed time, and the y-axis is optical output power. The measurement time was 1 minute. The standard deviation of the multimode WSLS output power was 0.1 dB compared to 0.03 dB for the new WSLS, indicating the better stability of the latter.

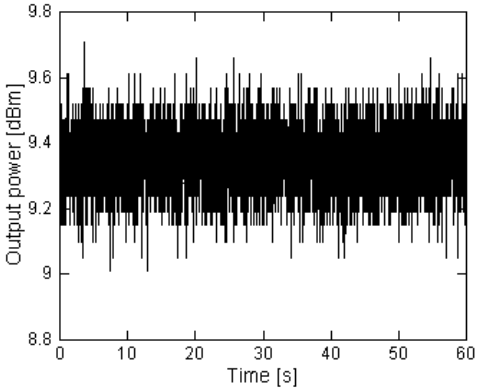

Figure 6 (a) Output power fluctuation for multimode WSLS at 1570 nm

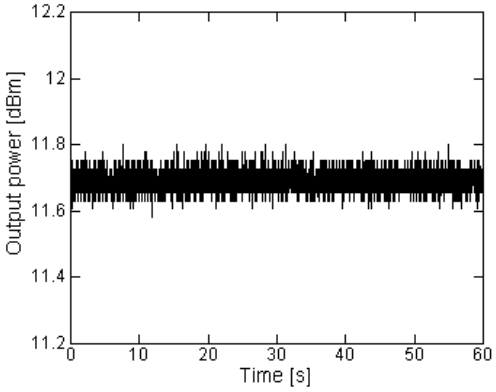

Figure 6 (b) Output power fluctuation for single-mode WSLS at 1550 nm

3.4 Evaluating Oscillation Spectrum Width during Sweeping

Next, we measured the oscillation spectrum width of this new WSLS during sweeping. Figure 7 shows the measurement setup. The output from the WSLS was input to a Fabry-Perot interferometer and the transmittance profile converted to an electrical signal at the optical receiver was observed with an oscilloscope to obtain an estimate of the oscillation spectrum width during sweeping. In the actual measurement, a trigger signal from the WSLS module is input to the oscilloscope to obtain synchronization and observe the transmittance profile from the Fabry-Perot interferometer converted to an electrical signal. The Fabry-Perot interferometer is composed of two flat-mirrors with a 90% reflection rate to obtain a free spectrum range of 250 pm and a finesse of 15. The optical receiver band is 50 MHz.

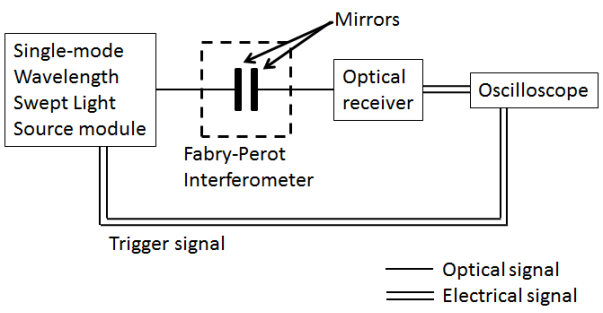

Figure 7 Spectrum width measurement setup

Figure 8 shows the transmittance profile observed with the oscilloscope. The x-axis is elapsed time and the y-axis is the transmitted optical power from the Fabry-Perot interferometer. The Fabry-Perot interferometer original transmittance spectrum width is calculated as about 16.7 pm (= 250 pm/15) from this free spectrum range and finesse, while as shown in Figure 8, a transmittance spectrum width of 23.4 pm was observed as calculated from the ratio with the free spectrum range and the transmittance spectrum width. The observed spectrum width is the sum of the Fabry-Perot interferometer original transmittance spectrum width and the oscillation spectrum width of this WSLS. Consequently, the oscillation spectrum width during sweeping of this WSLS can be estimated as about 6.7 pm (= 23.4 – 16.7 pm).

Based on the above results, this is WSLS has excellent optical output power stability and a narrow spectrum width, making it ideal for use in an FBG sensor monitor.

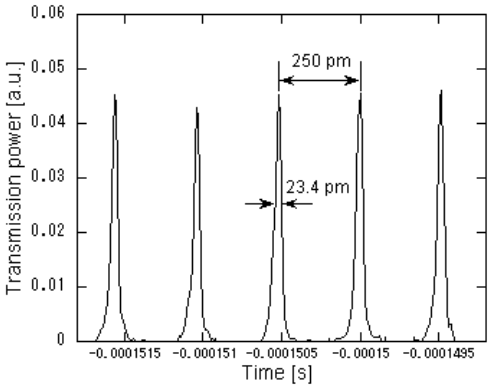

Figure 8 Transmission profile of Fabry-Perot interferometer

4 Development of FBG Sensor Monitor

4.1 Outline of FBG Sensor Monitor

We developed the FBG sensor monitor using this WSLS. Figure 9 shows the external appearance of the FBG sensor monitor. As shown in the figure, the AR4041A is a 4-port type to which separate FBG sensors can be connected for independent measurement at each port. However, we also developed the single-port AR4011A simultaneously.

Figure 9 External view of AR4041A FBG Sensor Monitor

Compared to our previously developed SF3041A/SF3011A, the WSLS module built into this new model is about 1/50th of the previous size. In addition, the signal processing circuits for controlling the WSLS and processing the measured data have also been greatly reduced in size. As a result, both the equipment weight and size have been reduced by about 40% compared to the previous model. This equipment is connected via a USB cable to the PC as in the previous model and an FBG sensor monitor system can be configured by connecting FBG sensors to the optical output ports.

We also developed the AR4042A program to control the equipment simultaneously. This control program runs on a PC to measure the reflected spectrum and the center wavelength, save the data, and measure the fiber length from the equipment to the FBG sensor. In addition, as a sample, we developed programs that display the reflected spectrum and center wavelength data, perform FFT analysis on the center wavelength data captured during each sweep and displays the results, and controls the AR4042A sending commands to the mapping file region of the PC, etc. Since these sample programs and program resources are open source, we hope customers will be easily able to incorporate the developed FBG sensor monitor into their existing systems.

4.2 Internal Structure of FBG Sensor Monitor and Measurement Principle

Figure 10 shows the internal structure of the AR4041A. The equipment is composed of a single-mode WSLS, optical coupler, optical circulator, optical receivers and signal processing circuit, etc. The optical output from

the WSLS module is split into four at the optical coupler, and after the optical signal passes through the optical circulator, is output to the FBG sensors arranged externally to the equipment. Light reflected back from the FBG sensors is passed once again through the optical circulator and converted to an electrical signal by the optical receivers. This electrical signal is amplified by a logarithmic amplifier to increase the dynamic range, and is then converted to a digital signal by sampling with an Analog to Digital Converter (ADC) before input to the signal processing circuits. The signal processing circuits calculate the wavelength differential from the reflection spectrum converted to this electrical signal and find the wavelength where this value is 0 as the center wavelength. This method for determining the center wavelength is very accurate because it is detected by computing the peak position of the reflected spectrum and it can be performed easily by digital processing using a Field-Programmable Gate Array (FPGA). This equipment sweeps 1250 times every second and supports high-speed sensing by calculating the position of the spectrum peak from the FBG sensor at every sweep, as well as the center wavelength using the waveform monitoring signal from the WSLS module.

The AR4011A features a higher optical output power because the light output from the WSLS is input to the optical circulator without splitting at the optical coupler. The optical output power of the AR4011A is +9 dBm ±4 dB compared to values of +2 dBm ±4 dB for the AR4041A.

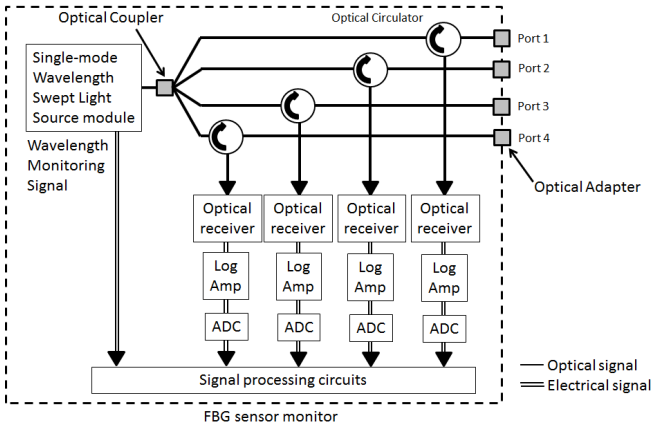

Figure 10 AR4041A FBG Sensor Monitor block diagram

4.3 Evaluating FBG Sensor Reflection Spectrum

Next, we evaluated the performance of this equipment. Since the WSLS built into this equipment has a narrow oscillation spectrum, it can measure the spectrum reflected from FBG sensors at much higher resolution compared to conventional model using multimode WSLS.

First, we observed the spectrum reflected from FBG sensors. Figure 11 shows the measurement setup. At measurement, 10 FBG sensors were connected in series with reflection wavelengths at every 5 nm as 1525, 1530, 1535, 1540, 1545, 1550, 1555, 1560, 1565, and 1570 nm. The light passing through all FBG sensors was reflected by the fiber end face. An optical terminator was connected to the fiber end face to prevent degradation of the dynamic range by the return to the equipment.

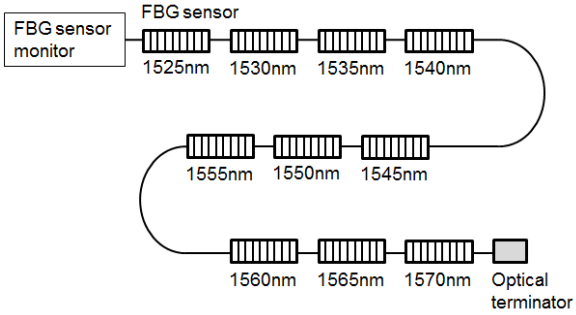

Figure 11 Measurement setup for reflection spectrum of FBG sensors

Figure 12 shows the spectrum reflected from the FBG sensors measured by the AR4011A. In addition to the main reflection spectrum from the 10 FBG sensors, a number of side lobes are shown.

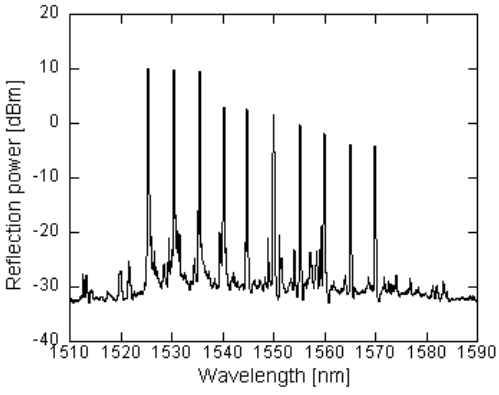

Figure 12 Reflection spectrum of FBG sensors

Figure 13 shows an expanded view of the spectrum reflected from the 1525-nm FBG sensor. Figure 13 (a) is the measurement result using the conventional SF3011A with a multimode WSLS, and Figure 13 (b) is the measurement result using the AR4011A with the single-mode WSLS. As shown in Figure 13 (a) using the conventional model, the spectrum width is 280 pm and, as well as a side lobe near 1525.5, there are shoulders on the left and right sides near –20 dBm. In contrast to this, the measurement result in Fig. 13 (b) shows a spectrum width of 220 pm, which is narrower than the result observed with the conventional model. Furthermore, although the shape is like a shoulder near –20 dBm as shown in Figure 13 (a), we can clearly see the side lobes near the peak in Figure 13 (b).

As described above, the measured spectrum width reflected from the FBG sensor is the sum of the original spectrum width of the FBG sensor and the oscillation spectrum width of the WSLS. As described in section 3.4, since the oscillation spectrum width during sweeping of the WSLS built into this model is 6.7 pm, we can note Figure 13 (b) broadly displays the original form of the spectrum reflected from the FBG sensor. Moreover, we can also note that the FBG sensor original reflection spectrum width is 213 pm (= 220 – 6.7 pm). In addition, the oscillation spectrum width of the multimode WSLS in the conventional model can be estimated as being about 67 pm (= 280 – 213 pm).

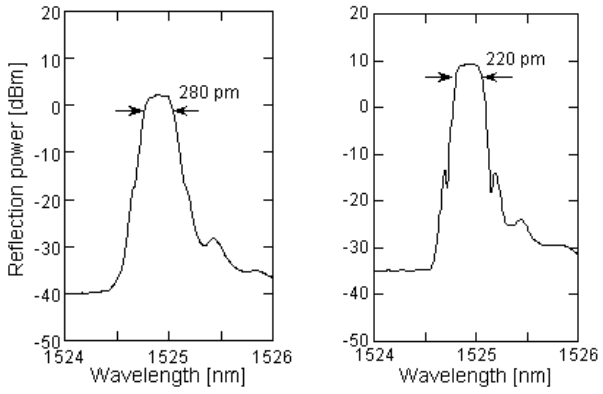

Figure13 Reflection spectrum of FBG sensor at 1525 nm
(a) Conventional FBG sensor monitor
(b) New FBG sensor monitor

4.4 Evaluating Wavelength Measurement Accuracy

Next, we evaluated the wavelength measurement accuracy of this equipment. As an example, we wrapped the FBG sensor in thermal insulating material to remove the effect of external heat and positioned it so that it was not subjected to any external forces and then measured the center wavelength of the reflected spectrum. Figure 14 shows the measurement results using the AR4011A for an FBG sensor with a reflected wavelength of 1550 nm. The x-axis is elapsed time and the y-axis is wavelength. The measurement time was 1 minute. The variation in the center wavelength measured under these conditions was caused by the equipment. In other words, it is the equipment wavelength observation accuracy. The standard deviation in the center wavelength over a 1-minute period was 0.08 pm. Consequently, the wavelength measurement accuracy of this equipment (wavelength repeatability) is 0.08 pm. This converts to a strain measurement accuracy of 0.064 με when using general-purpose FBG sensors (wavelength and strain conversion factor of 0.8 με/pm). Since the strain measurement accuracy of a conventional model is 2 to 3 με, we can note that we have achieved more than one order of magnitude better accuracy. Furthermore, since the measurement accuracy of a general electrical-type strain sensor is about 1 με, this system can also measure with 1-digit higher accuracy than electrical sensors.

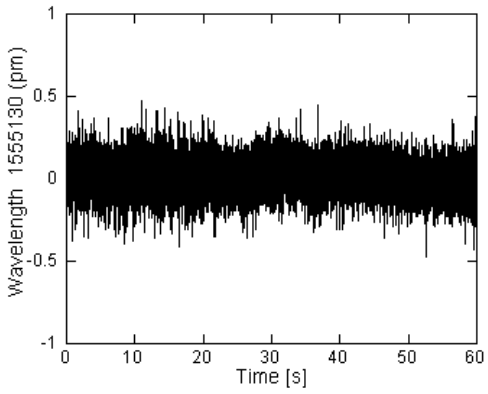

Figure 14 Wavelength fluctuation of center wavelength for FBG sensor at 1555 nm

Figure 15 shows the observed vibration when attaching a 1545-nm FBG sensor to the side of a tuning fork with a res-

onance frequency of 64 Hz. The x-axis is elapsed time and the y-axis is the wavelength difference from 1545 nm. It is possible to precisely observe the vibration attenuation behavior. This figure also shows an expanded view from elapsed time 38 s to 38.1 s where an amplitude of about 0.5 pm can be observed clearly.

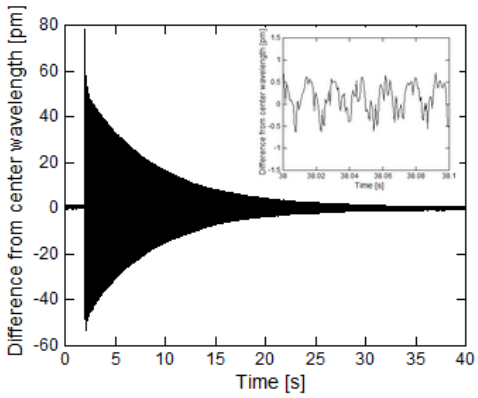

Figure 15 Result of vibration measurement at 1545 nm

5 Summary

We have developed an FBG sensor monitor using a single-mode WSLS with a sweep frequency of 1.25 kHz, and a wavelength sweep range of 110 nm and evaluated its characteristics.

First, we evaluated the characteristics of this WSLS. The output power wavelength dependency was small. After confirming the narrow oscillation spectrum width during sweeping, we developed the AR4041A/AR4011A FBG Sensor Monitor using this WSLS. In addition to having high responsivity of 1.25 kHz over the 80 nm between 1510 and 1590 nm, we also confirmed high measurement accuracy. As an example, we observed the spectrum reflected from FBG sensors and described a measurement accuracy of 0.08 pm. Converting this measurement result to strain measurement accuracy when using a general-purpose FBG sensor gave a measurement accuracy of 0.064με, which is at least one order of magnitude better than the previous conventional measuring equipment and electrical-type strain measurement equipment.

References

1) H. Iwaki, “Structural Health Monitoring for the building using FBG-based optical fiber sensors,” Proceedings of 47th Meeting on Lightwave Sensing Technology, LST47-15, 2011, in Japanese.
2) N. Kamiakito et al., Proceedings of 45th Meeting on Lightwave Sensing Technology, LST45-5, 2010, in Japanese.
3) M. IZUMO, and K. Matsuda, “Optocal water-level-sensor system using FBG,” Technical report of IEICE. OFT 104(700), 43-46, 2005-02-25, in Japanese.
4) E. Sugai et al., Japan Society of Civil Engineers Annual Meeting, pp.1431-1432, 2002, in Japanese.
5) H. Takeya, and T. Ozaki, “Application of FBG sensor to products in Mitsubishi Electric Corporation,” Proceedings of 37th Meeting on Lightwave Sensing Technology, LST37-16, 2006, in Japanese.
6) K. Fujihashi, T. Aoki, K. Okutsu, K. Arai, T. Komori, H. Fujita, Y. Kurosawa, Y. Fujinawa, and K. Sasaki, “Development of Seafloor Seismic and Tsunami Observation System , ” Underwater Technology, pp. 349-355, 2007.
7) T. Saitoh, K. Nakamura, Y. Takahashi, and K. Miyagi, “High-speed MEMS swept-wavelength light source for FBG sensor system,” 17th International Conference on Optical Fiber Sensors, Proceedings of SPIE Vol. 5855, pp.146-149, 2005.
8) T. Saitoh, K. Nakamura, Y. Takahashi, H. Iida, Y. Iki, and K. Miyagi, “Long-distance FBG sensor system using high-speed swept-wavelength light source,” in Proc. 18th International Conference on Optical Fiber Sensors (Cancun Mexico, October), ThE24 (2006).
9) T. Saitoh, "Optical spectrum analyzer and wavelength swept light source utilizing MEMS scanning mirrors," 7th Chitose International Forum on Photonics Science & Technology, 2006.
10) T. Saitoh, K. Nakamura, Y. Takahashi, H. Iida, Y. Iki, and K. Miyagi, “Ultra-Long-Distance Fiber Bragg Grating Sensor System,” IEEE Photonics Technology Letters, Vol. 19, No. 20, pp. 1616-1618, Oct. 2007.
11) Y. Takahashi, K. Nakamura, T. Saitoh, and H. Iida, “Development of High-speed FBG sensor monitor,” Anritsu Technical No.84, pp.28－33, 2007, in Japanese.
12) T. Saitoh, K. Nakamura, Y. Takahashi, H. Iida, Y. Iki, and K. Miyagi, “Ultra-long-distance (230 km) FBG sensor system," in Proc. 19th International Conference on Optical Fiber Sensors (Perth Australia, April), 70046C (2008).

13) T. Saitoh, "Ultra long distance FBG sensor system," The Pa-pers of Joint Technical Meeting on Light Application and Visual Science and Instrumentation and Measurement, IEE Japan, IM-08-1-1, 2008, in Japanese.

14) K. Nakamura, S. Morimoto, and T. Nakayama, "Single-Mode and Mode-Hop-Free Wavelength Sweep Light Source with Range of Over 160 nm and High Swept Frequency," IEEE Photonics Technology Letters, Vol. 22, No. 19, Oct. 2010.

Authors

Masaru Koshihara
Anritsu Devices Co., Ltd.
Sensing Equipment
Development Dept.

Kenichi Nakamura
Anritsu Devices Co., Ltd.
Sensing Equipment
Development Dept.

Noriaki Yamasaki
Anritsu Devices Co., Ltd.
Sensing Equipment
Development Dept.

Takanori Saitoh
Anritsu Devices Co., Ltd.
Sensing Equipment
Development Dept.

Hiroshi Furukawa
Anritsu Devices Co., Ltd.
Sensing Equipment
Development Dept.

Publicly available